CHEMISTRY AND CHEMICAL ENGINEERING

Volume 2024 | Number 3 Article 2

September 2024

ANTIBACTERIAL SEMI-FRITTED GLAZES CONTAINING IRON (III) AND MANGANESE (IV) OXIDES

Ivan A. LEVITSKIY
Belarusian State Technological University, Minsk, Belarus, levitskii@belstu.by

Mihail V. Dyadenko
Belarusian State Technological University, Minsk, Belarus, dyadenko@belstu.by

Ekaterina E. TRUSOVA
Belarusian State Technological University, Minsk, Belarus, trusova@belstu.by

ANTIBACTERIAL SEMI-FRITTED GLAZES CONTAINING IRON (III) AND MANGANESE (IV) OXIDES

Cover Page Footnote
This research was supported by the project X22UZB–023 funded by the Belarusian Repub-lican Foundation for Basic Research

ANTIBACTERIAL SEMI-FRITTED GLAZES CONTAINING IRON (III) AND MANGANESE (IV) OXIDES

Ivan A. LEVITSKII (levitskii@belstu.by)
Mihail V. DYADENKO (dyadenko@belstu.by)
Ekaterina E. TRUSOVA (trusova@belstu.by)
Belarusian State Technological University, Minsk, Belarus

The aim of this research work is production of colored antibacterial glaze coatings for ceramic products containing iron (III) and manganese (IV) oxides. The coatings are produced on the basis of multicalcium aluminoborosilicate frit, dolomite and iron or manganese oxides. The constant components in the raw mixture were feldspar, alumina, coal clay and kaolin. The coatings were obtained by finely grinding the components then applied to the dried semi-finished product and single fired at a temperature of 1200±5 °C for 60±2 minutes. The formation of the glaze layer, the decorative properties of coatings, and their physical and chemical and operational properties were examined. The structural features and phase composition of coatings have been studied. Antibacterial activity of coatings against Escherichia coli ATCC 8739 and Staphylococcus aureus ATCC 6538 test strains was determined.

Keywords: antibacterial activity, semi-fritted glaze, thermal expansion coefficient, heat resistance, wear resistance, chemical resistance

АНТИБАКТЕРИАЛЬНЫЕ ПОЛУФРИТТОВАННЫЕ ГЛАЗУРИ, СОДЕРЖАЩИЕ ОКСИДЫ ЖЕЛЕЗА (III) И МАРГАНЦА (IV)

Иван А. ЛЕВИЦКИЙ (levitskii@belstu.by)
Михаил В. ДЯДЕНКО (dyadenko@belstu.by)
Екатерина Е. ТРУСОВА (trusova@belstu.by)
Белорусский государственный технологический университет, Минск, Беларусь

Целью работы является получение цветных антибактериальных глазурных покрытий для керамических изделий, содержащих оксиды железа (III) и марганца (IV). Получение покрытий осуществлено на основе многокальциевой алюмоборосиликатной фритты, доломита и оксидов железа или марганца. В качестве постоянных составляющих в сырьевой смеси присутствовали полевой шпат, глинозем, глина огнеупорная и каолин. Покрытия получены тонким помолом составляющих с последующим нанесением на высушенный полуфабрикат и однократным обжигом при температуре 1200±5 °С при продолжительности 60±2 мин. Исследованы процессы формирования глазурного слоя, декоративные свойства покрытий, их физико-химические и эксплуатационные свойства. Изучены особенности структуры и фазового состава покрытий. Определена антибактериальная активность покрытий в отношении тест-штаммов Escherichia coli ATCC 8739 и Staphylococcus aureus ATCC 6538.

Ключевые слова: гомогенная антибактериальная активность, полуфриттованная глазурь, температурный коэффициент линейного расширения, термостойкость, износостойкость, химическая устойчивость

TARKIBIDA TEMIR (III) VA MARGANETS (IV) OKSIDLARI BO'LGAN ANTIBAKTERIAL YARIMFRITTA SIRLA

Ivan A. LEVITSKII (levitskii@belstu.by)
Mihail V. DYADENKO (dyadenko@belstu.by)
Ekaterina E. TRUSOVA (trusova@belstu.by)
Belarus davlat texnologiya universiteti, Minsk, Belarusiya

Ishning maqsadi: keramik buyumlar uchun temir (III) va marganets (IV) oksidlari bo'lgan rangli antibakterial sirli qoplamalarni olishdir. Qoplamalar ko'p kaltsiyli alumoborosilikatli fritta, dolomit va temir hamda marganets oksidlari asosida ishlab chiqilgan. Xom ashyolar aralashmasida doimiy komponentlar sifatida dala shpati, glinozyom, olovbardosh tuproq va kaolin mavjud. Qoplama mayin tuyilib so'ngra quritilgan yarim tayyor buyumga sepiladi va bir martalik kuydirish rejimida 1200±5 °C haroratda 60±2 daqiqa davomida pishirib olinadi. Sir qatlamini hosil qilish jarayonlari, qoplamalarning dekorativ hususiyatlari, ularning fizik-kimyoviy va ekspluatatsion hususiyatlari tadqiq qilindi. Qoplamaning asosiy strukturaviy tuzilishi va faza tarkiblari o'rganildi. Qoplamaning antibakterial faolligi Escherichia coli ATCC 8739 va Staphylococcus aureus ATCC 6538 test-shtammlari yordamida aniqlanai.

Kalit so'zlar: antibakterial faollik, yarim qovurilgan sir, termal kengayish koeffitsienti, issiqlikka chidamlilik, aşınma qarshilik, kimyoviy qarshilik

DOI: 10.34920/cce202432

Introduction

Better antibacterial properties of household items and construction products are a risk-free pressing issue for people and animals. In world practice, there are a large number of biocidal agents in the form of organic and inorganic compounds, including protective and decorative silicate coatings.

The aim of this research work was to obtain semi-fritted colored glaze coatings for porcelain stoneware in a wide range of brown colors with mixed-valent oxides Fe_2O_3 and MnO_2 with biocidal properties. Iron and manganese oxides are cheap and economically available materials widely used for coloring glasses, enamels and glazes. They can be used in large quantities ranging from 5.0 to 17.0 wt.% [1].

According to scientific literature sources and patents reviewed, these oxides can be used as antibacterial additives.

In this century, scientists started research on antibacterial properties of iron oxides. They found that magnetite ($FeO \cdot Fe_2O_3$) and maghemite (g-Fe_2O_3) exhibit antibacterial properties [2-4]. Hematite (a-Fe_2O_3) is also known to be antibacterially active [5-9]. The bactericidal activity of hematite

nanoparticles is due to the formation of oxygen-free radicals during the conversion of hydrogen peroxide into highly reactive hydroxyl radicals by the Fenton reaction. These free radicals act in many ways, such as depolymerization of saccharides or DNA strand breakdown, which ultimately leads to the death of bacteria according to reaction [10].

$$2H_2O + 2O_2^- \rightarrow H_2O_2 + O_2 + 2OH^-$$

$$Fe^{2+} + H_2O_2 \rightarrow Fe^{3+} + OH^-$$

The article [11] presents the findings of the antibacterial properties of nanocomposites of iron oxide and cobalt oxide due to their synergistic effect.

According to the research [12], there was a comparative study of the antibacterial action of iron and copper nanoparticles on clinical isolates of *Staphylococcus aureus*.

Iron nanoparticles were found to have a less multilateral effect compared to copper nanoparticles.

Manganese oxide is a cheap and economically available material. In its free form, it has a melting point of 535 °C and it is used to produce colored glaze coatings in a wide range of brown colors [13–15].

The oxidation of manganese oxide in the molten glaze depends on whether there are any oxidizing agents and reducing agents in the mixture, on the gas atmosphere of the furnace, on the heat treatment conditions and the composition of the glaze.

Manganese-containing glazes are widely used for decorating ceramic dishes, floor and wall tiles, stove tiles, etc. [16–21]. It should be noted that manganese oxide has been used in glaze compositions since ancient times [22–24]. There are, however, practically no studies on the antibacterial properties of manganese-containing glazes.

Research methods

Multicalcium frit based on system Na_2O–CaO–MgO–Al_2O_3–B_2O_3–SiO_2 in the amount of 20.0–32.5 wt.% was used as fritted component. The glass frit was melted at 1450 °C ± 10 °C in a gas glass melting furnace. The raw material mixture also included dolomite, feldspar, alumina, silica sand, kaolin and refractory clay. MnO_2 and Fe_2O_3 was individually used as additive, its amount varying 5.0–15.0 wt.%.

Sodium tripolyphosphate was used as an electrolyte in an amount of 0.20–0.25 wt.% introduced in excess of 100% of the components.

The glaze slurry was prepared by joint wet grinding of the components in the laboratory mill Speedy-1 (Italy) to the residue on sieve № 0063 in the amount of 0.4–0.6 wt.% raw material at 35–38% suspension humidity and glaze density of 1780–1820 kg/m^3.

A layer of glaze suspension was applied to semi-finished ceramic tiles with its subsequent drying at a temperature of 105±5 °C. Then the samples were fired in a fast mode in an industrial furnace at a temperature of 1200±5 °C for 60±2 minutes.

It was found that all the studied coatings had a high-quality glaze layer of matte texture with different colors depending on the content of coloring oxides Fe_2O_3 and MnO_2.

Color characteristics were determined according to the RAL color atlas [25].

The gloss of the glaze was assessed using black uviol glass on an FB-2 gloss meter.

The physical and chemical properties of coatings, including heat resistance, frost resistance, chemical resistance, wear resistance, etc., were studied according to the GOST 27180–2019 «Ceramic tiles» [26] and GOST 13996–2019 «Ceramic tiles. General specifications» [27] method.

The thermal expansion coefficient was determined using an electronic dilatometer DIL 402 PC (Netzsch, Germany) according to GOST 10978 –1983 [28].

The microhardness of the glaze layer was determined using a Wolpert Wilson (Germany).

The differential scanning calorimetric (DSC) measurements have been performed by DSC 402 (Netzsch, Germany). The heating range was up to 1200 °C at a speed of 3 K/min.

The crystal structure was investigated by X-ray diffraction (XRD) measurements using diffractometer D8 Advance (Brüker, Germany). The software DICVOL06 from FULLPROF package was used to calculate the lattice constants.

Using a scanning electron microscope JSM – 5610 LV (Japan), the structure of glaze coatings was studied.

The antibacterial activity of developed glazing coatings was researched at the Republican unitary enterprise «Scientific and Practical Center of Hygiene» accredited in the National system of accreditation of the Republic of Belarus in accordance with ISO 22196:2011 «Measurement of antibacterial activity on the surface of plastics and other non-porous materials» [29].

IR spectra of the glazes were taken using an IR spectrometer NEX – USTME.S. P (Thermo Nicolet, USA) in the range of 300–1400 cm^{-1}.

Results and Discussion

As-fired glaze coatings were characterized by a matte surface texture and a wide range of coating colors.

When Fe_2O_3 is introduced into the composition of the original transparent glaze, it gives a wide range of colors, predominantly of brown

tones. With the introduction of 5.0 wt.% of Fe_2O_3, color of coatings is predominantly olive-brown; with 7.5 wt.%, olive-brown and olive-green glazes are formed depending on the dolomite and frit amount. With 12.5 wt.% of Fe_2O_3, coatings are predominantly of olive tones, namely, they are olive green, dark olive and olive brown. Introduction 15.0 wt.% of Fe_2O_3 gives olive green and brown-green tones. The increased frit content in the composition of glazes leads to the darker tones, which is obviously due to its dissolution in the melt. Dolomite in glazes lightens the color, which is obviously due to the peculiarities of the coating crystallization processes.

Glazes containing MnO_3 are also characterized by brown tones. Here, it clearly depends more on the amount of MnO_2. At 5.0 wt.% of MnO_2, coatings of nut-brown, taupe and chocolate-brown tones are thus formed. At 7.5 wt.% of MnO_2, the color also varies between dark gray-brown, black-brown, chocolate brown. 10.0 wt.% additive of MnO_2 gives dark gray-brown, black-brown and black-olive tones to coatings. MnO_2 content in amounts of 10.0 and 15.0 wt.% gives a black-brown tone to glazes.

The studied characteristics of the decorative properties of coatings include the most important ones, which are the gloss indicators of glazes formed, in the studied systems of raw materials, by a matte surface that provides slip resistance. The gloss values of iron-containing coatings are 3–7%; the gloss values of manganese are 4–6%. The gloss indices slightly depend on the amount of introduced iron and manganese oxides, and they increase slightly as their content increases, instead of frit.

The thermal expansion coefficient of coatings for iron-containing compositions is in the range $(81.25–92.15)\cdot10^{-7}$ K^{-1}. Manganese-containning glazes have thermal expansion coefficient of $(79.05–89.04)\cdot10^{-7}$ K^{-1}. The ceramic base of the ceramic tiles used in the research, it was characterised by the thermal expansion coefficient of $82.2\cdot10^{-7}$ K^{-1}.

The dependence of the thermal expansion coefficient glazes on the content of coloring ox-

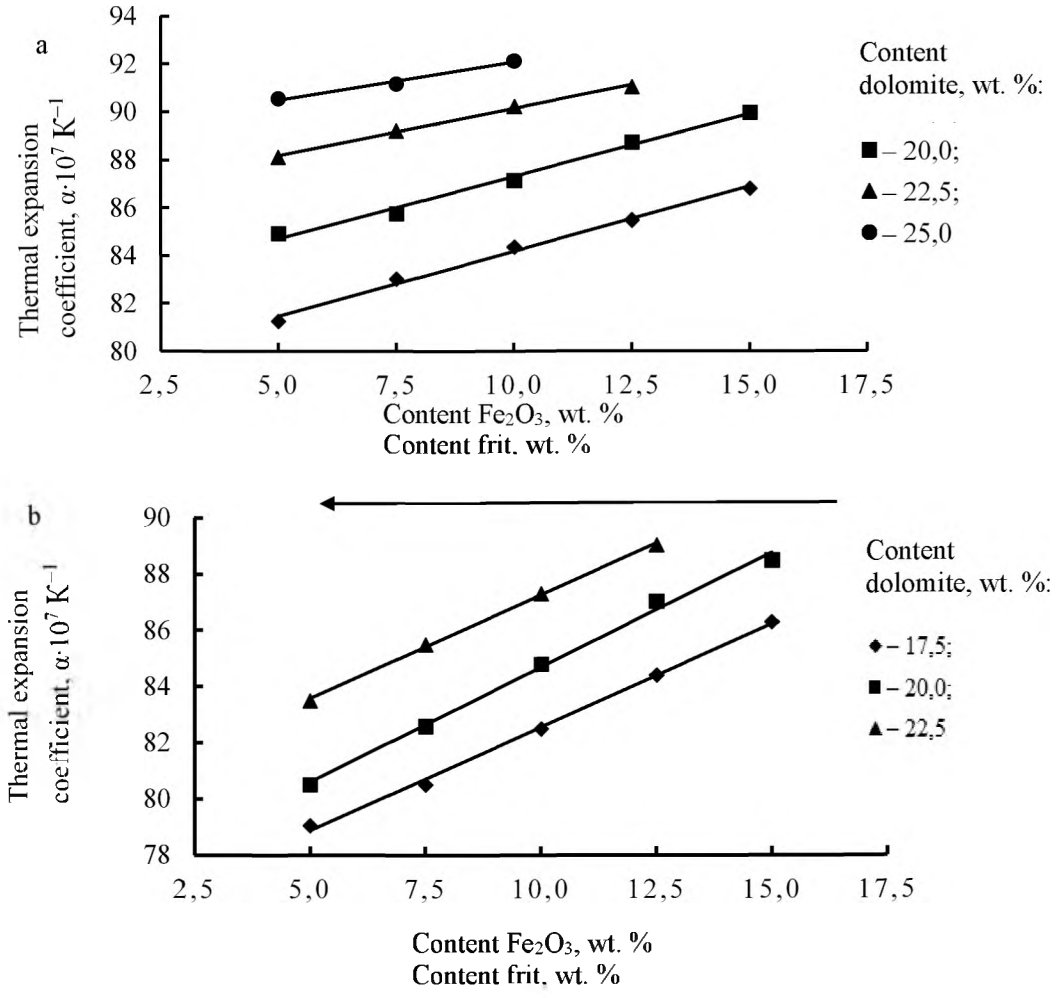

Figure 1. Dependence of the thermal expansion coefficient glazes on the content of coloring oxides Fe_2O_3 (a) and MnO_2 (b) introduced instead of frit.

ides Fe_2O_3 and MnO_2 introduced instead of frit is given on Figure 1.

As can be seen from Figure 1, thermal expansion coefficient of the synthesized glazes increase as the content of Fe_2O_3 and MnO_2 introduced individually instead of glass frit increases, which is obviously associated with their higher partial values of thermal expansion with the same original glaze composition, thermal expansion coefficient of which is $67.8 \cdot 10^{-7}$ K^{-1}. The glass frit used has thermal expansion coefficient values of $62.0 \cdot 10^{-7} K^{-1}$.

The thermal expansion coefficient is known to be determined by the strength and length of the connection between the structural elements and the force of interaction between them. Increased thermal expansion coefficient values of coatings with the introduction of Fe_2O_3 and MnO_2 indicates that there is an increase in these structural parameters.

The microhardness of glaze coatings is an important characteristic of the glaze layer and it is characterized by both the degree of coatings crystallization and the type of crystalline phases formed.

It was determined that the microhardness values of glazes with the introduction of Fe_2O_3 in an amount of 5.0 to 15.0 wt.% leads to the increased microhardness values of iron-containing coatings from 5008 to 6106 MPa, and from 5072 to 6147 MPa for manganese-containing coatings, i.e. these values are quantitatively very close.

Studies of heat and frost resistance of glaze coatings in accordance with GOST 27180 and the requirements of GOST 13996, which were respectively 150 °C and 100 cycles of alternating freezing and defrosting. In terms of wear resistance, the coatings belong to class 3, in terms of chemical resistance – to class GA; in terms of resistance to staining they correspond to class GA.

An analysis of the properties of the synthesized glazes is given in Table 1.

As can be seen from Table 1, the values of the physicochemical properties of iron and manganese-containing glazes are close and meet the standard. The antibacterial activity of iron-containing glazes is slightly higher than that of coatings containing MnO_2 to both strains studied.

As a result of studies of the X-ray phase composition of coatings, it was established that the synthesized iron-containing glazes as crystalline phases include hematite (α-Fe_2O_3) and maghemite (g-Fe_2O_3), as well as anorthite $Ca[Al_2Si_2O_8]$. Manganese-containing coatings are characterized by the presence of hausmannite ($MnO \cdot Mn_2O_3$, ramsdellite (MnO_2), as well as anorthite $Ca[Al_2Si_2O_8]$.

Differential scanning calorimetry (DSC) established the phase transformations observed in the raw mixtures during their heat treatment in the range of (20-1200)±0.1 °C for iron-containing

Table 1

Physico-chemical properties of synthesized glazes

Characteristics of the physico-chemical properties of synthesized glazes containing 7.5 wt.% Fe_2O_3 and MnO_2		
Parameter name	Glaze values	
	colored with Fe_2O_3	colored with MnO_2
Gloss values, %	3.7	6
Thermal expansion coefficient, $a \cdot 10^{-7}$, K^{-1}	84.94	84.8
Microhardness, MPa	5310	5756
Thermal stability, °C	150	150
Chemical resistance, class	Solution resistant № 1 and № 2 (class GA)	Solution resistant № 1 and № 2 (class GA)
Freezing resistance, cycles	100	100
Antibacterial activity of coatings against: *Escherichia coli* ATCC 8739 *Staphyloccocus aureus* ATCC – 6538	 1.09 ± 0.03 1.42 ± 0.03	 0.30 ± 0.03 1.15 ± 0.03

compositions containing 5.0 and 10.0 wt.% Fe_2O_3, given in Figure 2.

An endothermic effect of low intensity is observed with a minimum at 268.8 and 262.3 °C, associated with the dehydration of goethite impurities present in iron oxide (III) reacting to α-Fe_2O_3.

The endoeffect at 505.7 and 515.7 °C is caused by a part of α-Fe_2O_3 (hematite) reacting to γ-Fe_2O_3 (maghemite), and with minima at 574.0 and 573.2 °C – modification changes in quartz [30].

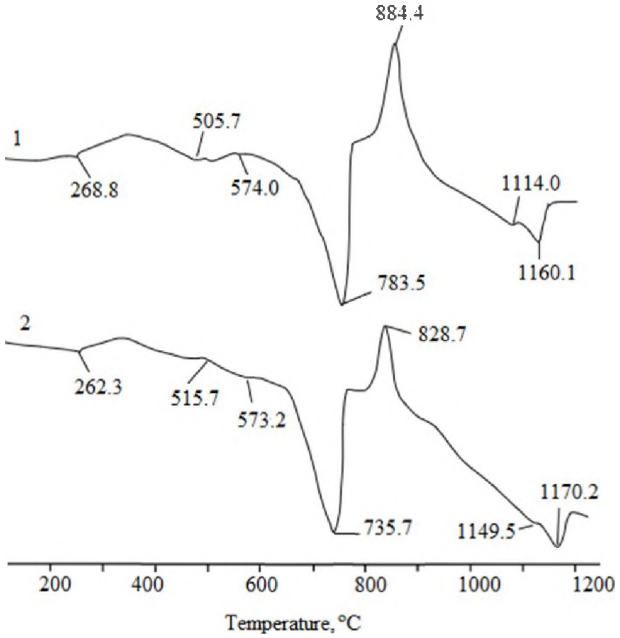

Figure 2. DSC curves for glaze containing Fe_2O_3, wt.%: 1 – 5.0; 2 – 10.0.

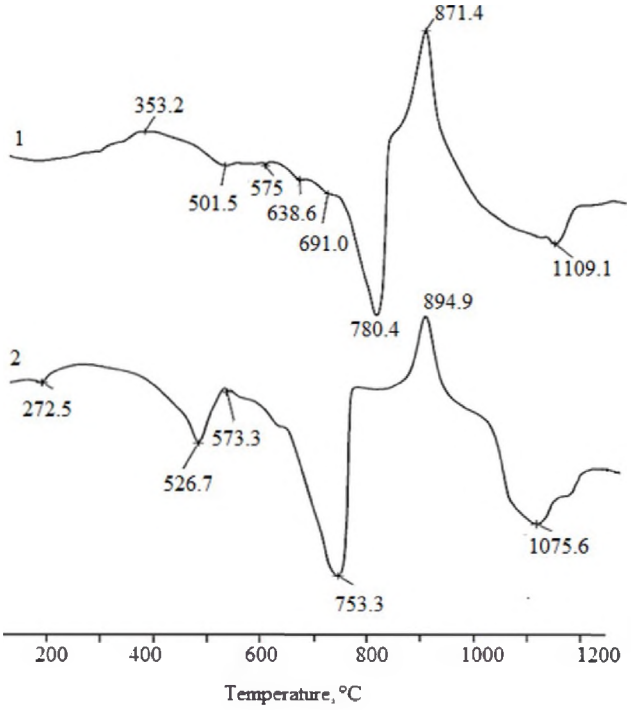

Figure 3. DSC curves for glaze containing MnO_2, wt.%: 1 – 5.0; 2 – 10.0.

The deep endothermic effect with a minimum at a temperature of 783.8 and 735.7 °C is due to the decomposition of dolomite with the formation of MgO and $CaCO_3$.

Exoeffects with a maximum at 884.4 and 828.7 °C are caused by the crystallization of anorthite, and the endoeffect at 1114.0 and 1149.5 °C is caused by the inverse γ-Fe_2O_3 (maghemite) transformation into α-Fe_2O_3 (hematite).

At 1160.1 and 1170.2 °C melting of the components of the glaze mixture occurs, which causes a shallow endothermic effect.

Manganese-containing glaze mixtures (Fig. 3) are characterized by a weak endo-effect with a minimum at a temperature of 272.5 °C, due to the removal of interlayer water from clay minerals.

The release of constitutional water from clay materials with partial restructuring is observed for the composition with 5.0 % MnO_2 at a temperature of 501.5 °C. Significantly deep endothermic effect with a minimum at 526.7 °C for composition with MnO_2 10.0 % is due to MnO_2 (pyrolusite) reacting to β-kurnakite (β-Mn_2O_3). A shallow, endothermic effect is observed with minima at 575 and 573.3 °C is due to the modified low-temperature quartz reacting to a high-temperature modification.

Endometrial effects of similar intensity with minima at 691 and 680 °C are due to the decomposition of pyrolusite with the formation of β-kurnakite β-Mn_2O_3 and α-hausmannite α-Mn_3O_4.

Deep endothermic effects with minima at 780.4 and 753.3 °C are caused by the decomposition of dolomite, and the formation of anorthite differs at 871.4 and 894.9 °C due to deep exothermic effects.

The melting temperature of the glaze mixtures is marked by an endo-effect with a minimum of 1109.1 (5.0 wt.% MnO_2) and decreases to 1075.6 °C (10.0 wt.% MnO_2). The reason for this decrease is the low melting point of MnO_2 (535 °C), which affects this process.

A weak endothermic effect with a minimum at 1133 °C for composition 2 can be caused by the reverse polymorphic transfor-

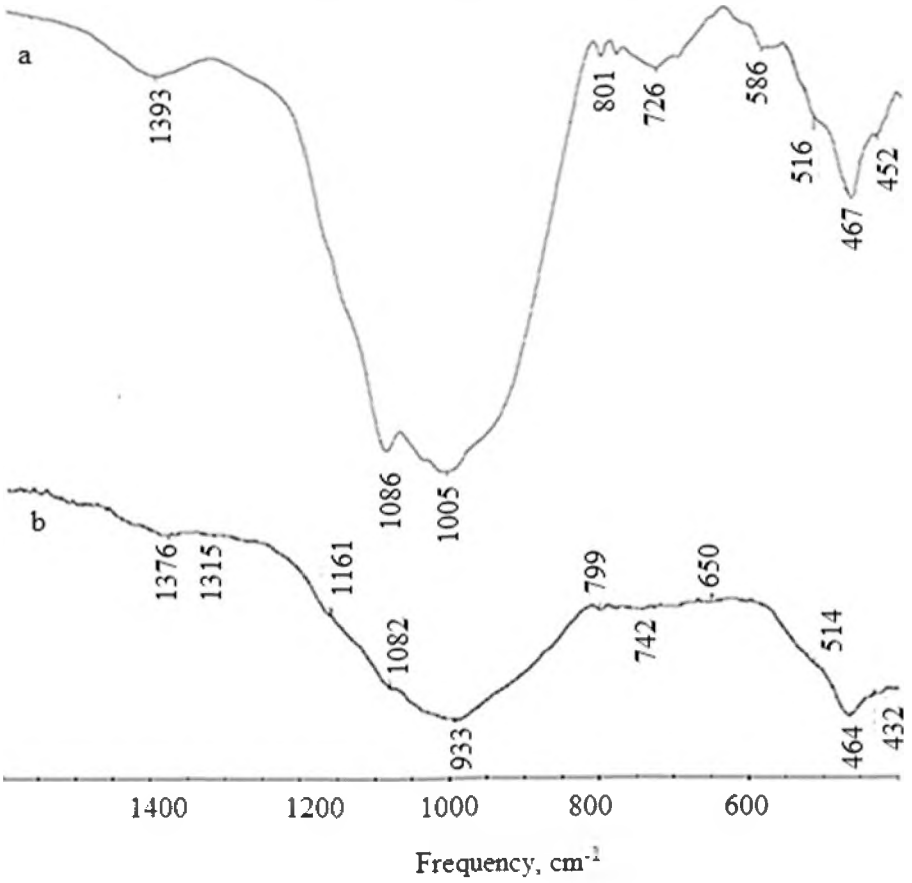

Figure 4. IR spectrum of glaze containing MnO_2 (a) and Fe_2O_3 (b).

mation of β-hausmannite into γ-hausmannite [30].

IR spectroscopy of optimal compositions of glazes containing 10 wt.% of Fe_2O_3 and MnO_2 made it possible to establish the formation features of the coating structure, which is illustrated in Figure 4.

The IR spectrum of iron-containing glaze is characterized by the following structure [31–32].

A low-intensity absorption band at 1376 cm^{-1} is specific to isolated $[BO_3]$ groups, which contribute to the glaze fusibility.

At 1315 cm^{-1}, a weak absorption band may be due to vibrations of three-coordinated boron in complexes with polymerized $[BO_3]$ groups, and at 1161 cm^{-1}, the maximum of the weak absorption band corresponds to the asymmetric stretching vibrations of the $[BO_3]$ groups.

The absorption band with a maximum at 1082 cm^{-1} is obviously the result of the superposition of bands caused by antisymmetric stretching vibrations of bridge Si–O–Si groups, as well as stretching vibrations of non-bridge $Si–O^-$ groups.

At 993 cm^{-1}, the broad absorption band is due to stretching vibrations of Si (Al)-O^- groups, and weak bands at 799 cm^{-1} -structural Si-O-Si groups, and at 742 cm^{-1} – stretching vibrations of Fe-O-(Fe) or Fe-O.

Absorption with a maximum at 650 cm^{-1} in the form of a shoulder may be due to vibrations of the Fe-O bond. Deformation vibrations of the O-Si-O groups are observed in the absorption band with a maximum at 464 cm^{-1}, and at 432 cm^{-1} are due to deformation vibrations of Si-O-Si groups.

A low-intensity absorption band in the high-frequency region at 1393 cm^{-1} is characteristic of isolated $[BO_3]$ groups, which contribute to an increase in the fusibility and spreadability of coatings.

The absorption band with a maximum at 1086 cm^{-1} is due to stretching vibrations of $Si-O^-$, and at 1005 cm^{-1} groups is due to Si(Al)-O^- groups.

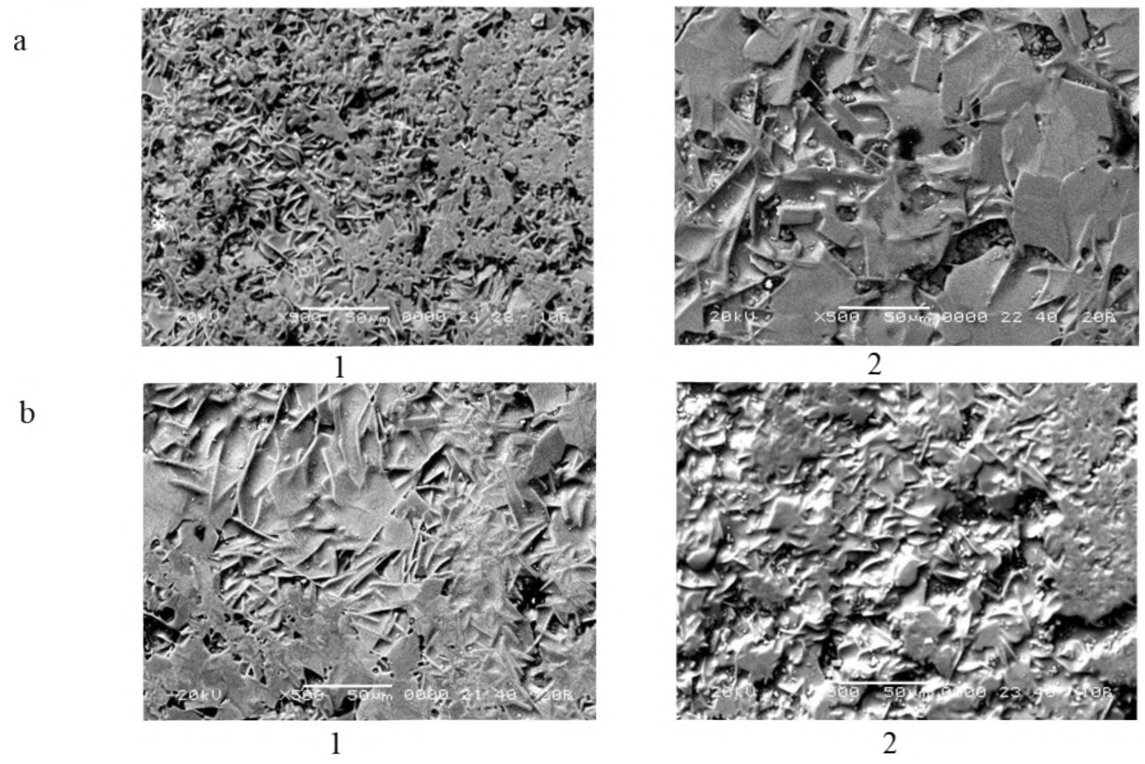

Figure 5. Electron microscopic images of glaze containing Fe_2O_3 (a) and MnO_2 (b), wt.%: 1 - 5.0; 2 - 10.0.

Stretching vibrations of structural Si-O-Si groups are characteristic of the absorption band with a maximum at 801 cm^{-1} and at 779 cm^{-1}, while at 726 cm^{-1} are stretching vibrations of Si-O-Al(Si) groups.

The absorption band with a maximum at 586 cm^{-1} is due to the six-coordinated aluminum in the glaze structure ([AlO_6] groups), and at 516 cm^{-1} may reflect vibrations of trigonal groups with B^{III}-O-B^{III} bonds, and the absorption band with a deep maximum at 476 cm^{-1} are deformation vibrations of O-Si-O groups, and at 452 cm^{-1} are of Si-O-Si groups.

Electron microscopic images made it possible to identify the structural features of the glaze coatings presented in Figure 5.

Electron microscopic examination determined that the chipped surface of glaze coatings is represented by crystalline and a small number of glassy phases. The iron-containing coating is characterized by high crystallization degree. The size of the crystals depends on the amount of Fe_2O_3 introduced and, with 5.0 wt.%, their size ranges from 20 to 50 μm. The structure is dominated by flattened crystals, evenly distributed over the surface. With an increase in the content of Fe_2O_3 10.0 wt.%, the predominantly plate-like crystals are formed, which significantly increase in size, reaching 50-80 μm. There are also areas of the glassy phase that occupy no more than 5% of the surface.

The manganese-containing coating is characterized by a high content of tabular crystals that are more elongated in one direction. Their size is from 3 to 40 μm in the largest dimension. There are also acicular crystals ranging from 0.5 to 40 μm in dimensions, located unevenly along the surface of the chip. The areas of vitreous component occupy no more than 10% of the coating surface. There are single isometric crystals with the dimensions of not more than 1 μm.

Conclusion

The possibility of obtaining colored semi-fritted glazes for porcelain stoneware of a wide range of colors, predominantly brown ones, was investigated due to the introduction of iron (III) and manganese (IV) oxide in the entire studied range of their content (5.0-15.0 wt.%).

The technological process of their use can be ensured by the existing operating technological equipment with adjustments to the technological regimes for preparing suspensions and firing coatings.

The developed compositions ensure the manufacture of porcelain stoneware in accordance with GOST 13996-2019. Glazes are antibacterially active against *Staphyloccocus aureus* ATCC 6538 and *Escherichia coli* ATCC 8739 strains.

The introduction of Fe_2O_3 and MnO_2 reduces coating gloss, and increases the thermal expansion coefficient and microhardness values, indicating the structural features of the formed coatings.

Acknowledgements

This research was supported by the project X22UZB–023 funded by the Belarusian Republican Foundation for Basic Research.

REFERENCES

1. Appen A.A. *Himiya stekla* [Glass Chemistry]. Leningrad. Chemistry Publ., 1970. 352.
2. Kong H., Song J., Jang J. One-step fabrication of magnetic γ-Fe_2O_3 / Polyrhodanine nanoparticles using in situ chemical oxidation polymerization and their antibacterial properties. *Chemical Communications*. 2010. 36, 6735–6737.
3. Chen T., Wang R., Xu L. Q., Neoh K. G., Kang En-T. Carboxymethyl chitosan-functionalized magnetic nanoparticles for disruption of biofilms of Staphylococcus aureus and Escherichia coli. *Industrial & Engineering Chemistry Research*. 2012. 51(40). 13164–13172.
4. Tran Nh., Mir A., Mallik D., Sinha A., Nayar S., Webster T. J. Bactericidal effect of iron oxide nanoparticles on Staphylococcus aureus. *Int J Nanomed*. 2010. 5. 277–283. DOI: 10.2147/ijn.s9220
5. Bhushan M., Kumar Y., Periyasamy L., Viswanath A. K. Antibacterial applications of α-Fe_2O_3/Co_3O_4 nanocomposites and study of their structural, optical, magnetic and cytotoxic characteristics. *Applied Nanoscience*. 2018. 8. 137–153.
6. Basnet P., Larsen G. K., Jadeja R. P., Hung Y.-C., Zhao Y. α-Fe_2O_3 nanocolumns and nanorods fabricated by electron beam evaporation for visible light photocatalytic and antimicrobial applications. *ACS Appl Mater Interfaces*. 2013. 5(6). 2085–2095.
7. Arakha M., Pal S., Samantarrai D., Panigrahi T. K., Mallick B. C., Pramanik K., Mallick B., Jha S. Antimicrobial activity of iron oxide nanoparticle upon modulation of nanoparticle-bacteria interface. *Sci Rep*. 2015. 5. 14813.
8. Rafi M.M., Ahmed K.S.Z., Nazeer K.P., Kumar D.S., Thamilselvan M. Synthesis, characterization and magnetic properties of hematite (α-Fe_2O_3) nanoparticles on polysaccharide templates and their antibacterial activity. *Appl Nanosci*, 2015. 5. 515–520.
9. Rudramurthy G. R., Swamy M. K., Sinniah U. R., Ghasemzadeh A. Nanoparticles: alternatives against drug-resistant pathogenic microbes. *Molecules*. 2016, 21 (7), 836. DOI: 10.3390/molecules21070836
10. Stankic S., Suman S., Haque F., Vidic J. Pure and multi metal oxide nanoparticles: synthesis, antibacterial and cytotoxic properties. *J. Nanobiotechnol*., 2016. 14. 73. DOI: 10.1186/s12951-016-0225-6
11. Touati D. Iron and oxidative stress in bacteria. *Arch Biochem Biophys*. 2000, 373(1). 1–6. DOI: 10.1006/abbi.1999.1518
12. Babushkina I.V., Borodulin V.B., Korshunov G.V., Puchinjan D.M. Comparative study of antibacterial action of iron and copper nanoparticles on clinical Staphylococcus aureus strains. *Saratov Journal of Medical Scientific Research*. 2010, 6(1). 11–14.
13. *Manganese glaze* Available at: https://ceramica-ch.ch/en/glossary/manganese-glaze. (accessed 23.06.2024)
14. Shen H., Yang J., Li J. High-temperature Ceramic Manganese Crystal Glaze. *Journal of Physics: Conference Series*. 2020. 1676. 012034–012038.
15. Molera J., Colomer M., Vallcorba O., Pradell T. Manganese crystalline phases developed in high lead glazes during firing. *Journal of the European Ceramic Society*. 2022, 43. 4006–4015. DOI:10.1016/j.jeurceramsoc.2022.03.028
16. Pradell T., Molina G., Molera J., Pla J., Labrador A. The use of micro-XRD for the study of glaze color decorations. *Applied Physics A*. 2013, 111(1). 121–127.
17. Pekkan K., Başkırkan H., Çakı M. Development of gold-bronze metallic glazes in a clay-based system for stoneware bodies. *Ceramics International*. 2018, 44(5), 4789–4794.
18. Chianga C.-Y, Greera H. F., Liub Ru-Sh Zhoua W. Formation, crystal growth and colour appearance of Mimetic Tianmu glaze. *Ceramics International*, 2016, 42(6), 7506–7513.
19. Coşkun N. D., Uz V., Issı A., Genç S., Çakı M. Effects of cooling interval and MnO_2, TiO_2, CdO, NiO additions on spheluritic willemite crystals. *Journal of Crystal Growth*, 2017. 458(15), 115–119.
20. *Insulator ultrahigh hardness brown glaze and preparation method thereof*. Patent CN, 106673441B, 2019.
21. *Matte metal glaze, matte metal glaze ceramic product prepared from same and preparation method of matte metal glaze ceramic product*: Patent CN, 105152685B, 2015.
22. Molera J., Coll J., Labrador A., Pradell T. Manganese brown decorations in 10th to 18th century Spanish tin glazed ceramics. *Applied Clay Science*, 2013. 82, 86–90.
23. Silvestri A., Nestola F., Peruzzo L. Manganese-Containing Inclusions in Late-Antique Glass Mosaic Tesserae: A New Technological Marker? *Minerals*, 2020, 10(10), 881. DOI: 10.3390/min10100881
24. Maggetti, M. SEM study of black, blue, violet and yellow inglaze colours of the oldest Swiss tin-opacified stove tiles. *Archaeometry*, 2021, 63(4), 727–737. DOI: 10.1111/arcm.12638.
25. *RAL color catalog*. Available at: https://colorscheme.ru/ral-colors/ral-classic.html. (accessed 23.06.2024).
26. GOST 27180 – 2019. Ceramic Tiles. Test. methods. Moskow, Stroyizdationform Publ., 2019, 58 (in Russ.)
27. GOST 13996 – 2019. Ceramic Tiles. General specifications. Moskow, Stroyizdationform Publ., 219. 42 (in Russ.)
28. GOST 10978 – 83. Inorganic glass and glass-ceramic materials. Method for determining the temperature coefficient of linedz expansion. Moscow, izdatel'stvo standartov Publ., 1983. 10 (in Russ.).
29. ISO 22196:2011. *Measurement of antibacterial activity on plastics and other non-porous surfaces*. Available at: https://www.iso.org/ru/standard/54431.html. (accessed 23.06.2024)
30. Ivanova V.P. *Termokhimicheskij analiz mineralov i gornykh porod* [Thermochemical analysis of minerals and rocks]. Leningrad, Nedra Publ., 1974. 399.
31. Plyusnina, I.I. *Infrakrasnyye spektry silikatov* [Infrared spectra of silicates]. Moscow, MSU Publ., 1967. 189.
32. Plyusnina, I.I. *Infrakrasnyye spektry mineralov* [Infrared spectra of minerals] Moscow, MSU Publ., 1977. 175.